Maximum-Likelihood Detection Performance of Uncoded OFDM in Impulsive Noise

Ahmed Mahmood, Mandar Chitre and Marc A. Armand
Department of Electrical and Computer Engineering, National University of Singapore, Singapore 117576
e-mail: {ahmed.mahmood, mandar, eleama}@nus.edu.sg

***Abstract*—Impulsive noise is a non-Gaussian heavy-tailed random process that is encountered in various communication scenarios. If not catered for, a single impulse will corrupt several symbols in an OFDM block. In this paper we analyze the maximum-likelihood (ML) detection error performance of uncoded OFDM. Results are presented for two different models with emphasis on binary and quadrature phase-shift keying (BPSK/QPSK) constellations. As the number of carriers increases, the error performance actually tends towards the Gaussian noise error curve irrespective of the noise impulsiveness. These results provide benchmarks to validate error performance of various schemes in impulsive noise.**

I. Introduction

Background noise is typically modelled (and rightly so) by a Gaussian process. This is a direct consequence of the central limit theorem (CLT) [1], [2]. In the literature, the performance of a digital communication scheme is usually ascertained for channels with additive white Gaussian noise (AWGN). However, the light-tailed Gaussian distribution is an ineffective fit for impulsive noise processes observed in various practical scenarios, such as powerline and underwater communication [3]–[5].

Several noise models have been used in the literature to simulate impulsive noise. Notable mentions are the Middleton models [6], the Gaussian-Bernoulli-Gaussian (GBG) channel [7]–[9] and the additive white symmetric α-stable noise (AWSαSN) process [4], [10], [11]. The Middleton and GBG models have the advantage of being based on closed-form density functions. The AWSαSN process is derived from heavy-tailed symmetric α-stable (SαS) density functions, which along with their Gaussian counterpart, share the stability property [12], [13]. Supported by the generalized central limit theorem (GCLT), the AWSαSN channel represents a logical model for impulsive noise. Further still, it simulates practical impulsive noise extremely well.

In our previous work, we have highlighted the effect of impulsive noise (modelled as AWSαSN) in single-carrier communication systems with emphasis on phase shift keying (PSK) [10], [11]. Statistical analysis of the noise process was thoroughly conducted after conversion to its complex baseband form. Conventional matched-filter conversion warrants the resulting noise to be heavy-tailed and isotropic. Under some rules and modification to the passband-to-baseband conversion mechanism, the in-phase and quadrature components of the resulting noise can have independent and identically distributed (IID) components. This provides significantly better maximum-likelihood (ML) detection performance over the conventional conversion case. These results open up a number of worthy problems including its application and analysis to multicarrier systems, which is the purpose of this paper.

Orthogonal frequency-division multiplexing (OFDM) has garnered significant attention from the research community these last few decades. Modern day multicarrier systems are increasingly being incorporated with OFDM as it provides a number of advantages in terms of implementation and performance over other digital modulation schemes [1], [14]. High spectral efficiency, low inter-symbol interference (ISI) due to a guard interval, single-tap equalization and efficient implementation via the fast Fourier transform (FFT) algorithm are some of its attractive properties. The effects of impulsive noise on an OFDM system are established and well-known [8]. At the receiver, an N-point FFT is invoked on the received vector to generate the OFDM symbol block. The same operation would cause an impulse in the noise vector to be mapped onto an N-point complex sinusoid that affects all symbols in the OFDM block. Therefore, the *transformed* noise vector will have dependent components. As the FFT is a linear operation, multiple impulses in the noise vector will result in a summation of sinusoids with varying frequencies and amplitudes in the transformed noise vector. The frequency and amplitude of each of these sinusoids depend on the corresponding impulse location and weight, respectively, in the original noise vector.

A number of well-written articles discuss methods to mitigate this effect. The most applied concept is noise cancellation. Though sub-optimal, this is a valuable technique. In a practical OFDM system, a few symbols are reserved as nulls and pilots due to various constraints. Taking advantage of this, conceptual similarities between the OFDM transmit-receive equation and the syndromes in a block code are highlighted in [8], [9]. Reed-Solomon codes are then used to exploit the information in these symbols to estimate the noise with good effect. Similarly in [15], the authors have employed the relatively new concepts of compressed sensing along with efficient and robust convex programmes developed in [16] to estimate the noise. The quoted articles focus on the GBG noise model and inherently assume the application of a passband-to-baseband conversion mechanism (like the one in [10]) that preserves the impulsiveness of the noise. In all impulsive noise cancellation techniques the objective is to remove (cancel) the impulses from the received vector so that

Gaussian detection/decoding may be performed.

This paper focuses on an entirely new problem: Analyzing the performance of ML detection in OFDM for a channel contaminated with AWSαSN. A passband-to-baseband conversion mechanism as that in [10] is employed. The simulation results surprisingly depict that the error rates achieved *approach* the Gaussian error curve as the number of carriers increase. The results can be used as benchmarks for various schemes developed to mitigate impulsive noise.

This manuscript is divided as follows: In Sthe channection-II we present the notation and concepts used in this paper. Detection schemes and design considerations are discussed in Section-III. We present and discuss the novel results in Section-IV and conclude the article in Section-V.

II. Notations and Concepts

A. SαS Variables & Vectors

The SαS family of distributions, as the name suggests, share two defining properties:

1) *Symmetry:* If X is a random variable and $f_X(x)$ its probability density function (PDF), then X is *symmetric* if $f_X(x) = f_X(-x)$. Extending this to random vectors, we see that $\vec{X}$ is symmetric if $f_{\vec{X}}(\vec{x}) = f_{\vec{X}}(-\vec{x})$.
2) *Stability:* The GCLT states that the PDF of a sum of K independent and identically distributed (IID) random variables (or vectors) converges to a *stable* distribution as $K \to \infty$. By this definition the Gaussian distribution is also stable with the added constraint of finite variance.

A univariate SαS PDF is parametrized by the characteristic exponent $\alpha \in (0, 2]$ and the scale parameter $\delta \in (0, \infty)$. We therefore denote the distribution of the corresponding random variable by $\mathcal{S}(\alpha, \delta)$. Apart from the zero-mean Gaussian $\mathcal{S}(2, \delta)$ and zero-median Cauchy $\mathcal{S}(1, \delta)$ instances, SαS PDFs cannot be expressed in analytic form [12], [13]. Fortunately, the characteristic function (CF) $\Phi_X(\theta)$ exists in closed form and can be alternatively used to statistically characterize X:

$$\Phi_X(\theta) = E[e^{j\theta X}] = \exp\left(-\delta^\alpha |\theta|^\alpha\right) \tag{1}$$

where $E[\cdot]$ is the expectation operator.

Non-Gaussian SαS distributions have algebraic tails and are thus heavy-tailed. If $X \sim \mathcal{S}(\alpha, \delta)$ where $\alpha \neq 2$, then

$$f_X(x) \approx \left(\frac{\alpha\delta^\alpha \sin(\pi\alpha/2)\Gamma(\alpha)}{\pi}\right)|x|^{-\alpha-1} \tag{2}$$

as $|x| \to \infty$. Here, $\Gamma(\cdot)$ denotes the gamma function. As $\alpha \to 0$ the tails become increasingly heavier, thus making the outcomes more impulsive. From (2), we observe that second-order moments of X are infinite. One can validate these observations from the Cauchy PDF below:

$$f_X(x) = \frac{\delta}{\pi(x^2 + \delta^2)}. \tag{3}$$

The multivariate CF of any N-dimensional SαS random vector $\vec{X}$ is given by

$$\Phi_{\vec{X}}(\vec{\theta}) = E\left[e^{j\vec{X}^T\vec{\theta}}\right] \exp\left(-\int_{S_N} |\langle\vec{\theta}.\vec{s}\rangle|^\alpha \Gamma(\vec{s}).d\vec{s}\right) \tag{4}$$

where S_N represents all points on the $(N-1)$-dimensional unit circle lying in N-dimensional space and $\langle\cdot\rangle$ denotes the inner product of two vectors [12]. Here, $\Gamma(\vec{s})$ is the *spectral measure* and is defined over $\vec{s} \in S_N$. It is equal for *any two* antipodal vectors $\vec{s}$, i.e., $\Gamma(\vec{s}) = \Gamma(-\vec{s})$, and assigns weights to $|\langle\vec{\theta}, \vec{s}\rangle|^\alpha$. In (4), the integration is performed over all points $\vec{s} \in S_N$.

To better understand the relationship between $\Gamma(\vec{s})$ and the configuration of an SαS PDF, we briefly discuss two special cases:

1) The Isotropic Case: If $\vec{X}$ is an N-dimensional isotropic SαS vector with each component $\mathcal{S}(\alpha, \delta)$, its CF is given by

$$\Phi_{\vec{X}}(\vec{\theta}) = \exp\left(-\delta^\alpha \|\vec{\theta}\|^\alpha\right). \tag{5}$$

The CF is solely a function of the magnitude of the frequency domain vector $\vec{\theta}$ [12]. For the isotropic case, $\Gamma(\vec{s})$ is constant over all $\vec{s} \in S_N$. □

2) IID Components: If $\vec{X}$ is an N-dimensional SαS vector and its components are IID copies of $X \sim \mathcal{S}(\alpha, \delta)$, the joint-CF is given by the multiplication of N individual copies of the expression in (1):

$$\Phi_{\vec{X}}(\vec{\theta}) = \exp\left(-\delta^\alpha \left(\sum_{i=1}^{N} |\theta_i|^\alpha\right)\right). \tag{6}$$

Here, $\Gamma(\vec{s})$ is non-zero only for a finite number of $\vec{s} \in S_N$. Precisely, it is a sum of N-dimensional equal-weighted Dirac delta functions located at the Cartesian axis intercepts with the $(N-1)$-dimensional unit circle. An example is the univariate SαS case, which in essence is a 1-dimensional random vector with a single $\mathcal{S}(\alpha, \delta)$ distributed component. In this case $S_1 = \{-1, 1\}$ and $\Gamma(s) = \delta^\alpha/2(D(s-1) + D(s+1))$ where $D(s)$ is the Dirac delta function.

Any *linear transformation* of an SαS random vector is SαS as well. Further still, $\Gamma(\vec{s})$ will be non-zero for discrete $\vec{s} \in S_N$ only if the corresponding $\vec{X}$ can be represented as a linear combination of an SαS vector with IID components [12]. We exploit this property later on in Section-III. □

From these examples, it is clear that there is a *unique* relationship between the PDF structure and the spectral measure of an SαS random vector. Just as one can interpret aspects of a time domain signal from its Fourier transform and vice-versa, the same can be accomplished for $\Gamma(\vec{s})$ and its PDF (albeit under a different set of rules). Though the CF in (4) is defined for a real valued $\vec{X}$, it can be extended easily to the complex case by noting that any N-dimensional complex vector can be expressed as a $2N$-dimensional real vector.

B. AWSαSN

AWSαSN has been used in the literature to model an impulsive noise process [10], [17]. For $\alpha = 2$ it reverts to the well-known additive white Gaussian noise (AWGN) model. As non-Gaussian SαS variables lack finite second-order moments, the power spectral density (PSD) of an AWSαSN process is infinite. Thus, contrary to the Gaussian case, 'whiteness' does not imply a flat PSD for non-Gaussian AWSαSN. However,

the term is kept to signify that samples of the noise process are IID and share a joint-CF of the type in (6).

C. The Channel Model

In an N-carrier OFDM system, the baseband transmit-receive equation is given by

$$\vec{y} = H_c A^H \vec{x} + \vec{n} \tag{7}$$

where H_c is the circular channel-state matrix and A is the unitary inverse discrete Fourier transform (IDFT) matrix. Both H_c and A are of dimension $N \times N$. We denote the i^{th} column of A as $\vec{a}_i$. The model consists of zero-Doppler and Rayleigh block fading. The use of a cyclic prefix and a sufficient-length guard interval is assumed. The N-dimensional vectors $\vec{y}$, $\vec{x}$ and $\vec{n}$ represent the received symbols, transmitted OFDM block and noise, respectively. All elements in (7) are complex. The OFDM symbol set is finite and denoted by $\mathcal{X}$, i.e., $\vec{x} \in \mathcal{X}$. The size of the per-carrier constellation is M, which implies $|\mathcal{X}| = M^N$. We may rewrite (7) in terms of the equivalent expression:

$$\vec{y} = A^H H \vec{x} + \vec{n} \tag{8}$$

where $H = \text{diag}(h_1, h_2, \ldots, h_N)$ and $h_i \sim \mathcal{CN}(0, \sigma_h^2)\ \forall\ i \in \{1, 2, \ldots, N\}$.

Practical systems assign nulls and pilots within an OFDM block due to various design/channel constraints. Therefore, $\vec{x}$ is considered to be partially composed of these symbols [14]. Other techniques such as forward error correction, time/frequency interleaving and reduction of the peak-to-average power ratio (PAPR) are typically employed to enhance OFDM performance. As our goal is to analyze the ML performance in impulsive noise at the baseband level, these schemes are considered as independent problems and are not discussed in this paper.

In AWSαSN, the complex noise vector $\vec{n}$ can take on a plethora of statistical configurations due to the passband-to-baseband conversion process [10], [11]. For example, conventional matched-filter conversion results in an isotropic PDF [10]. However, ML detection in isotropic impulsive noise is known to have poor performance [10]. The passband-to-baseband conversion may be modified while maintaining its linearity to provide more exploitable statistical configurations of $\vec{n}$. One such mechanism, initially proposed in [10], introduces passband sampling along with certain constraints on design parameters to generate $\vec{n}$ with IID components. The real and imaginary parts of each element are also IID. In essence the components of $\vec{n}$ are samples of (what we define as) a *complex* AWSαSN process. This configuration *guarantees* the best error performance over all possible baseband noise PDFs. Thus, for the remainder of this paper we assume $\vec{n}$ to be a non-Gaussian complex AWSαSN vector with $\mathcal{S}(\alpha, \delta_n)$ real and imaginary components.

In [10], the performance of single-carrier phase-shift keying in complex AWSαSN was analyzed. Large error performance gains were achieved by exploiting the baseband PDF via rotated constellations. The optimal rotation angle and performance gain depends on the employed constellation. If this scheme were to be extended to the multicarrier case, the symbols on every carrier would have to be rotated by a certain angle. For the purpose of comparison, we will also show a few results for the case of no fading and near-optimal rotation. The channel model for this is

$$\vec{y} = A^H A_\phi \vec{x} + \vec{n} \tag{9}$$

where $A_\phi = \text{diag}(e^{j\phi_1}, e^{j\phi_2}, \ldots, e^{j\phi_N})$ and ϕ_i is the rotation angle for the i^{th} carrier $\forall\ i \in \{1, 2, \ldots, N\}$. From (9), we observe that $A_\phi \vec{x}$ is the *transmitted* OFDM symbol and therefore the receiver will have full knowledge of A_ϕ.

In (9), the optimal rotation angles are functions of the signal-to-noise ratio (SNR), the per-carrier constellation pattern, the number of carriers and the noise impulsiveness. Evaluating a suitable A_ϕ may not be feasible as practical channels introduce a random phase to each carrier via fading. This is mathematically characterized by H in (8). Also, transferring channel information to the transmitter is usually not an option. This problem is augmented by the fact that the channel may change by the time H is estimated and delivered. Further still, calculation of the optimal angle is computationally very complex. On the bright side, the range of angles for which the system performs at near-optimum levels is large and most *random* instances of A_ϕ will offer good performance with high probability. As we will see later, the performance gain as N increases does not warrant the cost of calculating the optimal A_ϕ.

A more appropriate approach would allow analyzing the *average* error rates over all possible combinations of H in (8) and A_ϕ in (9). From a practical point-of-view, this would provide a benchmark for the error performance of any instance of H the channel introduces or a random A_ϕ.

III. Optimization Techniques and ML Detection

One key attribute of $\vec{n}$ is that its joint-PDF will have *tails* directed along each Cartesian axis in both the positive and negative directions. To observe this, we present the pdf for the single-carrier ($N = 1$) Cauchy case in Fig. 1. Here, x_1 and x_2 denote the real and imaginary components of $\vec{n}$, respectively, and are IID standard Cauchy random variables. The tails are clearly visible. For values of α near 2, the tails are still visible but less pronounced than those in Fig. 1.

A strong result from the discussion in Section-II is that the $\Gamma(\vec{s})$ corresponding to $\vec{n}$ is non-zero only when $\vec{s}$ is directed along each positive and negative Cartesian axis. In other words, there are $4N$ unique vectors $\vec{s} \in S_{2N}$ and their respective weights $\Gamma(\vec{s})$ that completely characterize the statistics of $\vec{n}$. We denote the set of these vectors by S_T. The relationship between the PDF's tails and $\vec{s} \in S_T$ is very clear: The tails are directed along the vectors in S_T. If $\vec{X}$ has a CF of the form in (6), then any linear mapping of $\vec{X}$ results in a similar transformation in the tails of its PDF, and hence the vectors in S_T. The example below depicts the tail transformation of an SαS random vector under linear mapping:

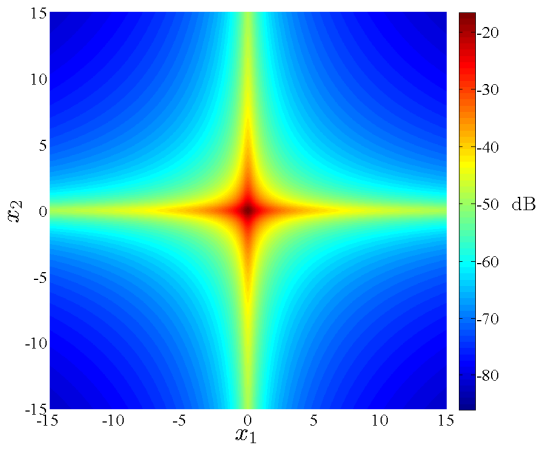

Fig. 1. Top view of the standard Cauchy bivariate PDF. X_1 and X_2 are IID with distribution $\mathcal{S}(1,1)$.

1) Example: Let $\vec{Y} = B\vec{X}$, where $\vec{Y}$ and $\vec{X}$ are real N-dimensional SαS vectors with IID components and B is a real $N \times N$ matrix with its i^{th} column denoted by $\vec{b}_i$. Then

$$\begin{aligned}\Phi_{\vec{Y}}(\vec{\theta}) &= \Phi_{\vec{X}}(B^T\vec{\theta}) \\ &= \Phi_{\vec{X}}(\vec{\theta}) = \exp\left(-\delta^\alpha\left(\sum_{i=1}^{N}|\vec{b}_i^T\vec{\theta}|^\alpha\right)\right). \end{aligned} \quad (10)$$

On comparison with (4) and (6), we observe that $\Gamma(\vec{s})$ consists of a finite sum of Dirac delta functions located at $\vec{s}_i = \pm\vec{b}_i/\|\vec{b}_i\|$ with weight $\delta^\alpha\|\vec{b}_i\|/2 \ \forall \ i \in \{1,2,\ldots,N\}$. The weight of each transformed tail is proportional to $\|\vec{b}_i\|$. If B is invertible then the number of tails in the PDF of $\vec{Y}$ is the same as that of $\vec{X}$. □

We know that an impulse in $\vec{n}$ affects all symbols in $\vec{x}$ after the FFT operation. From a statistical perspective, this phenomenon is represented by the tails in the PDF of $H^{-1}A\vec{n}$ and $A_\phi^H A\vec{n}$ in (8) and (9), respectively. With suitable values of ϕ_i in (9), the tail vectors S_T of the baseband noise PDF (shifted to $A^H A_\phi\vec{x}$) do not point directly towards any other OFDM constellation point [10]. One may use a geometric approach using S_T and the OFDM constellation to accomplish this. However, we derive A_ϕ by minimizing a cost function based on the error probability (EP).

The ML detection rule for (9) given $\vec{x}$ is transmitted is

$$\begin{aligned}\hat{x} &= \arg\max_{\vec{x}\in\mathcal{X}} f_{\vec{Y}|\vec{X}=\vec{x}}(\vec{y}|\vec{x}) \\ &= \arg\max_{\vec{x}\in\mathcal{X}} f_{\vec{N}}(\vec{y} - A^H A_\phi\vec{x}) \\ &= \arg\max_{\vec{x}\in\mathcal{X}} \prod_{i=1}^{N} f(y_i - \vec{a}_i^H A_\phi\vec{x}) \end{aligned} \quad (11)$$

where $f(\cdot)$ denotes the *bivariate* PDF of any complex component of $\vec{n}$. If the OFDM symbols are equiprobable, the error probability for the detection scheme in (11) is given by

$$\text{EP}(A_\phi) = \frac{1}{M^N}\sum_{j=1}^{M^N}\int_{\vec{y}:\hat{x}\neq\vec{x}_j}\prod_{i=1}^{N} f(y_i - \vec{a}_i^H A_\phi\vec{x}_j)d\vec{y} \quad (12)$$

The integration is performed over all $\vec{y}$ such that $\hat{x} \neq \vec{x}_j$ where $\vec{x}_j \in \mathcal{X}$ is the transmitted OFDM symbol. The expression in (12) is not solvable as the integration is performed over complex areas. This is augmented by the fact that $f(\cdot)$ is not available in closed form with the exception of the Cauchy case and averaging needs to be performed over *all* transmitted symbols $\vec{x} \in \mathcal{X}$. On the other hand, by extrapolating the results of [10], the ML error performance for (11) is almost constant (near-optimal) for a large range of ϕ_i at high SNR. Thus evaluating the optimal A_ϕ at every SNR instance does not provide adequate gain. Therefore A_ϕ may be evaluated just once for a given SNR where error performance meets requirements.

Calculating A_ϕ from (12) is not trivial and requires further simplifications. We propose minimizing the following cost function:

$$J(A_\phi) = \sum_{j=1}^{M^N}\prod_{i=1}^{N}\sum_{l=1,l\neq j}^{M^N} f\left(\vec{a}_i^H A_\phi\left(\vec{x}_l - \vec{x}_j\right)\right). \quad (13)$$

Observe that $J(\cdot)$ is a normalized version of EP$(\cdot)$ with the detection regions limited to the points $\vec{y} = \vec{a}_i^H A_\phi\vec{x}_l$ where $l \neq j$. The expression in (13) is convex and can be minimized via conventional techniques such as gradient descent. However, this is still very complex to solve for large N. Though many sub-optimal schemes may be designed to evaluate A_ϕ, it is a different problem which will not be pursued in this paper.

Following the expression in (11), the ML detection rule for (8) given $\vec{x}$ is transmitted is

$$\hat{x} = \arg\max_{\vec{x}\in\mathcal{X}} \prod_{i=1}^{N} f(y_i - \vec{a}_i^H H\vec{x}). \quad (14)$$

In the Gaussian case, evaluating (11) and (14) is equivalent to individually performing ML (Euclidean) detection on each carrier. The complexity of this technique is proportional to N [1]. However, for the general SαS case, the complexity increases exponentially with N. Though indeed difficult to calculate, we depict results and trends for a small number of carriers and extrapolate these results to schemes with a larger number carriers.

IV. Simulations

Before presenting simulation results, we briefly comment on the SNR measure employed in our analysis. Following [10], [11], [17], the SNR is evaluated by

$$\text{SNR} = \frac{d^2\sigma_h^2}{4m\delta_n^2} \quad (15)$$

for (8) and

$$\text{SNR} = \frac{d^2}{4m\delta_n^2} \quad (16)$$

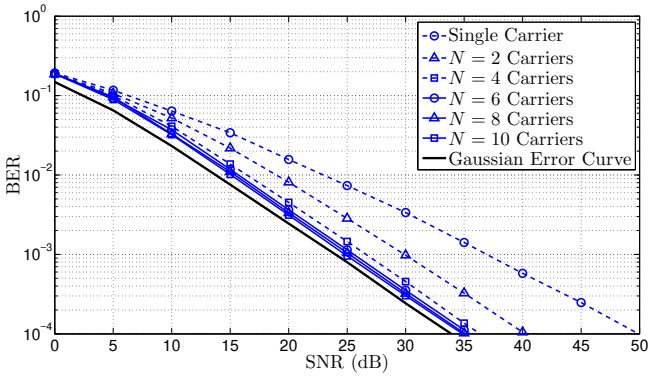

Fig. 2. Bit error rates averaged over H with Cauchy $\vec{n}$ in (8). The curves are generated for various N with per-carrier constellation BPSK.

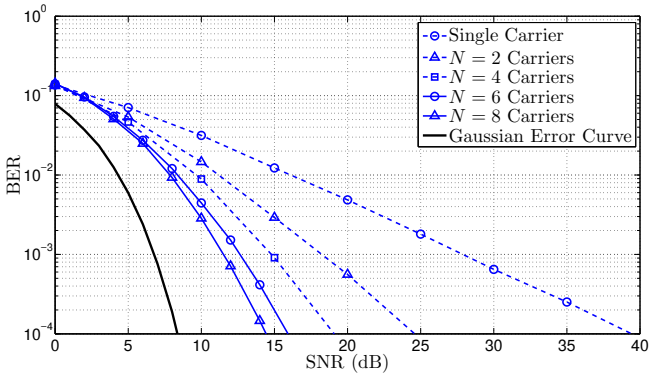

Fig. 4. Bit error rates for various N with Cauchy $\vec{n}$ in (9). The per-carrier constellation is BPSK and A_ϕ is optimized for SNR= 20dB.

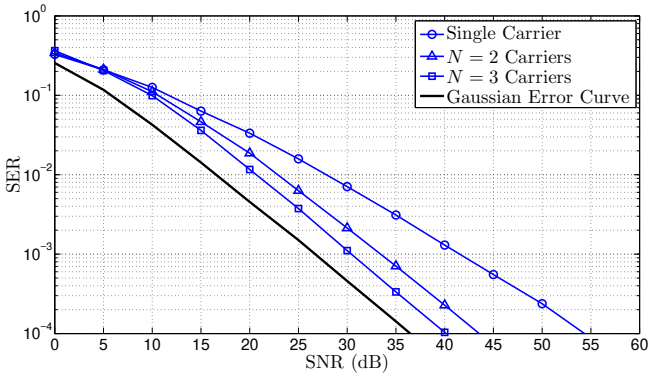

Fig. 3. Symbol error rates averaged over H with Cauchy $\vec{n}$ in (8). The curves are generated for various N with per-carrier constellation QPSK.

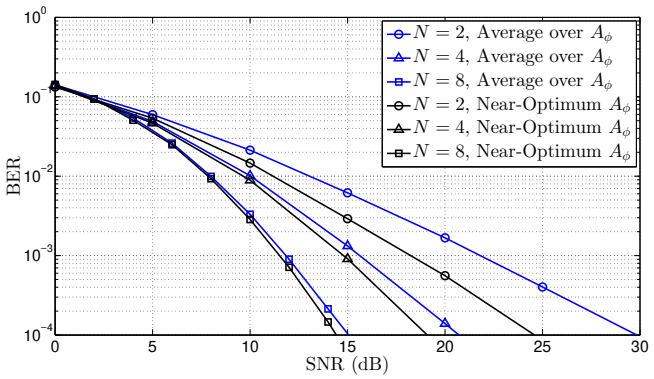

Fig. 5. Bit error rates averaged over A_ϕ with Cauchy $\vec{n}$ in (9). The curves are generated for various N with per-carrier constellation BPSK.

for (9). Here, d^2 and m represent the average signal power per-carrier and the number of information bits per symbol, respectively. In either case, the SNR converges to the SNR-per-symbol (E_s/N_0) when $\vec{n}$ is circular symmetric complex Gaussian. The relationship between the SNR in (16) with the passband AWSαSN process is presented in [18] and highlights design considerations for the passband-to-baseband conversion process for the SαS framework.

All simulations and analysis are conducted for Cauchy $\vec{n}$. The Cauchy distribution shares the heavy-tailed property common to all non-Gaussian SαS distributions. Thus, results for this case can be intuitively extended to all other cases [10]. The simulations are conducted via the Monte Carlo method. At least 4000 errors are accumulated for BER/SER$< 10^{-3}$ and 1000 errors otherwise.

In Fig. 2 we present bit error rate (BER) curves for the model in (8). The per-carrier constellation is binary phase-shift keying (BPSK) and $\vec{n}$ is a Cauchy complex AWSαSN vector. The BER is averaged over all possible instances of H and the receiver is assumed to have full knowledge of the channel. It is observed that the error rates *tend towards* the Gaussian error curve as N increases. We see a similar trend for the symbol error rate (SER) in Fig. 3 when the per-carrier constellation is quadrature phase-shift keying (QPSK). Though not presented here, similar convergence is expected of other constellations. Due to the complexity of ML detection, generating error plots for larger values of N is not possible, yet the convergence phenomenon can still be very much appreciated from the figures.

Intuitively, we know that the information within an impulse is scattered over a large bandwidth. This will be *larger* than the available bandwidth per-carrier. Increasing N essentially allows the scheme to access a larger bandwidth. In fact, the increase in bandwidth is directly proportional to N. This allows the detection process to harness more noise information and thus enhance performance in non-Gaussian AWSαSN. Increasing N in AWGN does not improve error performance as the noise information that affects any sub-carrier is constrained to the latter's bandwidth. According to this reasoning, one can expect the detection performance in impulsive noise to *converge* to a certain level when *sufficient* information is harnessed. This, in turn, is accomplished by increasing the OFDM symbol bandwidth (and therefore N).

For the model in (11), we present results in Fig. 4 for the Cauchy case with per-carrier constellation BPSK. We evaluate A_ϕ at SNR$=$ 20dB for each scheme by minimizing (13) via gradient descent. The error performance is then calculated over all SNR values with the same A_ϕ. As with Fig. 2, the error

performance becomes better with increasing N. This trend however is more pronounced in Fig. 4.

Though A_ϕ significantly influences the error performance in the single-carrier case [10], the range of values for which it performs well enhances with increasing N. We plot the *average* BER over all possible values of A_ϕ for $N = 2,\ 4$ and 8 in Fig. 5. For comparison, the near-optimal error curves in Fig. 4 corresponding to these values of N are redrawn in Fig. 5. We note that as the number of carriers increase, the difference between the near-optimal and average error performance decreases substantially. Thus the probability of a *random* A_ϕ producing near-optimal error performance in PSK increases with N. This phenomenon is more pronounced for the fading model in Figs. 2 and 3 as the *instances* of H that offer optimal error performance cannot exceed the Gaussian error curve and yet perform better than the curves averaged over H. This leaves a very minute performance gain over the averaged curves.

V. Conclusion

In this paper, we have investigated the performance of ML detection for uncoded OFDM in impulsive noise which is modelled as samples of a complex AWSαSN process. Novel results show that the error performance improves substantially by increasing the number of carriers in an OFDM system. This is shown for channels without fading and Rayleigh block fading. In a pure AWSαSN scenario, the rotation angle has a significant influence in the single-carrier case [10], [11]. We show that the optimal rotation angle need not to be evaluated for large carrier schemes. In fact any random rotation may offer near-optimal error performance with high probability.

For both models in (11) and (14), the trends encountered in the BPSK and QPSK cases also apply to other commonly used constellations. Similarly, the performance in Cauchy noise may be intuitively extended to all other noise scenarios with varying impulsiveness [10].

Noise cancellation techniques are commonly employed to combat impulsive noise due to their implementability [15]. Though complex to evaluate, ML detection performance can be used as a benchmark for schemes designed to mitigate the effect of impulsive noise. From our results, we state that the Gaussian error curve may be used as the optimal benchmark for large carrier OFDM schemes contaminated by impulsive noise. This is more pronounced for the case of Rayleigh block fading in (14).

References

[1] J. Proakis and M. Salehi, *Digital Communications*, ser. McGraw-Hill higher education. McGraw-Hill Education, 2007.

[2] A. Papoulis and U. S. Pillai, *Probability, Random Variables and Stochastic Processes*. Boston: McGraw-Hill, Dec 2001.

[3] M. Zimmermann and K. Dostert, "Analysis and modeling of impulsive noise in broad-band powerline communications," *Electromagnetic Compatibility, IEEE Transactions on*, vol. 44, no. 1, pp. 249 –258, Feb 2002.

[4] M. Chitre, J. Potter, and S.-H. Ong, "Optimal and near-optimal signal detection in snapping shrimp dominated ambient noise," *Oceanic Engineering, IEEE Journal of*, vol. 31, no. 2, pp. 497 –503, April 2006.

[5] M. Chitre, J. Potter, and O. S. Heng, "Underwater acoustic channel characterisation for medium-range shallow water communications," in *OCEANS '04. MTTS/IEEE TECHNO-OCEAN '04*, vol. 1, Nov. 2004, pp. 40 –45.

[6] D. Middleton, "Non-Gaussian noise models in signal processing for telecommunications: new methods and results for class A and class B noise models," *Information Theory, IEEE Transactions on*, vol. 45, no. 4, pp. 1129–1149, May 1999.

[7] M. Ghosh, "Analysis of the effect of impulse noise on multicarrier and single carrier QAM systems," *Communications, IEEE Transactions on*, vol. 44, no. 2, pp. 145–147, Feb. 1996.

[8] F. Abdelkefi, P. Duhamel, and F. Alberge, "Impulsive noise cancellation in multicarrier transmission," *Communications, IEEE Transactions on*, vol. 53, no. 1, pp. 94–106, Jan. 2005.

[9] ——, "A necessary condition on the location of pilot tones for maximizing the correction capacity in OFDM systems," *Communications, IEEE Transactions on*, vol. 55, no. 2, pp. 356–366, Feb. 2007.

[10] A. Mahmood, M. Chitre, and M. A. Armand, "PSK communication with passband additive symmetric α-stable noise," *Communications, IEEE Transactions on*, vol. 60, no. 10, pp. 2990 –3000, Oct. 2012.

[11] ——, "Improving PSK performance in snapping shrimp noise with rotated constellations," in *Proceedings of the Seventh ACM International Conference on Underwater Networks and Systems*, ser. WUWNet '12, no. 12, New York, NY, USA, 2012, pp. 1–8.

[12] G. Samorodnitsky and M. S. Taqqu, *Stable Non-Gaussian Random Processes: Stochastic Models with Infinite Variance*. Chapman & Hall, 1994.

[13] C. L. Nikias and M. Shao, *Signal processing with Alpha-Stable Distributions and Applications*. New York: Chapman-Hall, 1996.

[14] H. Schulze and C. Lueders, *Theory and Applications of OFDM and CDMA: Wideband Wireless Communications*. Wiley, 2005.

[15] G. Caire, T. Al-Naffouri, and A. Narayanan, "Impulse noise cancellation in OFDM: an application of compressed sensing," in *Information Theory, 2008. ISIT 2008. IEEE International Symposium on*, July, pp. 1293–1297.

[16] E. Candes and P. Randall, "Highly robust error correction byconvex programming," *Information Theory, IEEE Transactions on*, vol. 54, no. 7, pp. 2829–2840, July 2008.

[17] M. Chitre, J. Potter, and S. Ong, "Viterbi decoding of convolutional codes in symmetric α-stable noise," *Communications, IEEE Transactions on*, vol. 55, no. 12, pp. 2230 –2233, Dec. 2007.

[18] A. Mahmood, M. Chitre, and M. A. Armand, "Baseband characterization of additive white symmetric α-stable noise," in *Global Telecommunications Conference (GLOBECOM 2012), 2012 IEEE*, Dec. 2012, pp. 3696–3701.